

## Photoelectron satellite structure from the 3*d* and 4*d* inner-shell ionization of rubidium and cesium: Role of atomic relaxation

S. Fritzsche,<sup>1,2,\*</sup> K. Jänkälä,<sup>2</sup> M. Huttula,<sup>2</sup> S. Urpelainen,<sup>2,3</sup> and H. Aksela<sup>2</sup>  
<sup>1</sup>*Gesellschaft für Schwerionenforschung (GSI), D-64291 Darmstadt, Germany*  
<sup>2</sup>*Department of Physical Sciences, P.O. Box 3000, 90014 University of Oulu, Finland*  
<sup>3</sup>*Max-lab, Lund University, Box 118, SE-22100 Lund, Sweden*  
 (Received 14 July 2008; published 10 September 2008)

The photoelectron satellite structure of rubidium and cesium has been investigated following the photoionization of an  $nd$  ( $n=3,4$ ) inner-shell electron. The intensity ratios of the  $nd^{-1}ms$  monopole and  $nd^{-1}m'p$  conjugated satellite lines have been measured at MAX-lab by using high-resolution electron spectroscopy. For rubidium, moreover, the energy dependence of the  $3d_j6s/3d_j5s$  and  $3d_j5p/3d_j5s$  intensity ratios with  $j=3/2$  and  $5/2$  is measured and compared with multiconfiguration Dirac-Fock calculations. A good or at least reasonable agreement is found for both the monopole and conjugated shake-up probabilities if the relaxation of the bound-state electron density is taken into account in the computation of the photoionization cross sections. It is shown that, for the inner-shell ionization of medium and heavy atoms, the orbital relaxation accounts for a significant part of the satellite structure in the photoelectron spectra.

DOI: 10.1103/PhysRevA.78.032514

PACS number(s): 33.60.+q, 32.80.Fb

### I. INTRODUCTION

Atomic photoionization along with high-resolution electron spectroscopy has been found to be a powerful technique for studying many-electron effects in atoms and molecules. Beside the main photoelectron peaks, which can typically be understood within the atomic shell model of independent electrons, the satellites to these peaks often display a very rich structure and are known to provide insight into the role of atomic correlations. These satellites reflect both the fine structure of the photoion as well as the probability of the target to remain in an excited ionic state after the photoelectron has left the atom. From the energy dependence of these satellites in photoelectron and (subsequent) Auger spectra, moreover, useful information was drawn about the electron-electron correlations for different shell structures of atoms and ions [1–3]. Therefore, measurements of the photoelectron satellites also help explore the capabilities of present-day atomic theory and, in particular, how well the conjugated shake-up process can be treated by the many-electron atomic codes available today.

For atoms with one and two electrons outside of otherwise closed shells, the photosatellites from the inner-shell ionization have been explored in great detail [4–12]. These investigations showed that the shake-up and shake-off processes must be treated as multielectron phenomena for which the bound-state and continuum interactions have to be taken properly into account. In the electron spectra, these shake-up processes are seen as satellites at the low-kinetic-energy side of the main peaks. For the sake of simplicity, however, the main experimental and theoretical emphasis has been placed so far on the satellite lines of lithium, following its  $1s$  photoionization. For lithium, a large number of experimental [3–5,13] and theoretical [5,14] case studies have been carried

out for both the partial cross sections and the asymmetry parameters for the angular distribution of the diagram and satellite lines. Moreover, high-resolution measurements were made also for the  $1s2p^1P$  and  $1s2p^3P$  conjugated shake-up satellite lines in order to analyze a process in which the valence electron does exchange not only energy but also angular momentum with the photoelectron. In particular, the populations of the  $^1P$  and  $^3P$  states have found considerable interest because, owing to the conservation of the spin in the electron-photon interaction, the  $^3P$  term is populated by a pure  $\langle 1s|\epsilon s\rangle$  monopole transition [4,15]. Despite the great progress in describing the lithium  $1s$  photosatellites, the comparison of high-resolution measurements with advanced  $R$ -matrix [5,14] and many-body computations [16] shows various discrepancies and makes it clear that our present understanding of the electronic correlations is still far from being complete, even for a simple system such as lithium and, especially, if the bound-state density couples to the electron continuum.

Although lithium provides a great “playground” for developing the many-electron theory for the photoionization of atoms, the medium and heavy alkali-metal atoms are also of interest for exploring relativistic effects in the electron-photon interaction as well as for their use in photoelectric cells or as a catalyst in chemical processes and in different compounds (e.g., [17,18]). For Rb and Cs, especially, the near degeneracy of the  $4d$ ,  $4f$ , and  $5d$  electrons leads to rather complex photoionization and subsequent Auger spectra that are rich in configuration mixing and shake-up [10,19] processes. For these atoms, so far, only the monopole shake-up was analyzed qualitatively by exploiting the overlap of the one-electron orbitals as calculated in different self-consistent-field (SCF) procedures [10,20]. Any many-particle treatment of these atoms that incorporates all internal correlations and the continuum interaction is therefore much more elaborate to carry out and will require the development of more advanced codes than presently available [21].

\*s.fritzsche@gsi.de

In this work, we report on a high-resolution measurement of the photoelectron satellite structures of rubidium and cesium following the (photo)ionization of a  $3d$  and  $4d$ , respectively, inner-shell electron. For these photoelectrons, the intensity ratios of the  $nd^{-1}ms$  monopole and  $nd^{-1}m'p$  conjugated satellite lines have been measured at MAX-lab at fixed energy well above the threshold. For rubidium, in addition, the photon energy dependence of the  $3d_{5/2}/3d_{3/2}$  and  $3d_{5/2}p/3d_{3/2}p$  intensity ratios with  $j=3/2, 5/2$  have been recorded and are compared with multiconfiguration Dirac-Fock calculations. Reasonable to good agreement is found for both the monopole and conjugated shake-up probabilities if the relaxation of the bound-state electron density due to the photoemission of the inner-shell electron is taken into account. This computational model has the great advantage that no distinction need be made for the conjugated shake-up transitions despite the different correlation contributions that lead to these shake-up lines.

In the next section, we briefly describe the experiments, carried out at the MAX-lab undulator beamline I411. The theoretical framework and computations are later discussed in Sec. III with emphasis on how the rearrangement of the electron density is included in calculating the photoionization amplitudes and cross sections. In Sec. IV, we then present and discuss the  $3d \rightarrow nl$  satellite spectrum of rubidium and the  $4d \rightarrow n'l'$  spectrum of cesium. For rubidium, moreover, the energy-dependent branching ratios are discussed. Finally, a few conclusions are given in Sec. V.

## II. EXPERIMENT

The experiments were conducted at the MAX-II 3rd generation synchrotron storage ring in MAX-laboratory (Lund, Sweden), utilizing the undulator beamline I411 dedicated for gas-phase studies. The electron spectra were recorded using a rotatable modified Scienta SES-100 electron kinetic energy analyzer (for further details, see Ref. [19]). The (angle-independent) intensities of the main and satellite peaks were measured at the magic angle of  $54.7^\circ$  with respect to the polarization plane of the synchrotron radiation.

The beam of atomic vapor was produced by using a resistively heated oven at a temperature of  $115^\circ\text{C}$  for Rb and  $92^\circ\text{C}$  for Cs. The total experimental broadening from the photon energy bandwidth and analyzer contribution was about  $100\text{ meV}$  for both samples, which is approximately the same as the lifetime broadening of the  $3d$  and  $4d$  ionized states of Rb and Cs, respectively. Special care was taken to avoid the blending by Auger lines that occurs at some fixed kinetic energies. When such an overlap with Auger lines was unavoidable, the region was measured with slightly different photon energy and the intensity from the Auger lines was subtracted during the data analysis.

The binding energy calibration for the Cs  $4d$  photoelectron spectrum was obtained from the Xe  $4d_{3/2}$  and  $4d_{5/2}$  binding energies [22]. The transmission behavior of the hemispherical analyzer (in a constant pass mode) as a function of the kinetic energy was determined experimentally by using the constant ratio of the Xe  $4d_{3/2,5/2}$  photoelectron lines and the  $\text{N}_{4,5}\text{O}_{2,3}\text{O}_{2,3}$  Auger lines, as described in Ref. [23].

## III. THEORY AND COMPUTATIONS

Several theoretical models have been proposed and utilized in the past in order to include many-electron effects beyond the frozen-core Hartree-Fock (HF) model in the computations of photoionization cross sections and electron intensities. These models include the configuration interaction (CI) and multiconfiguration Hartree-Fock (MCHF) and Dirac-Fock (MCDF) methods, and many-body perturbation theory, as well as the  $R$ -matrix approach. They all aim to efficiently describe the atomic (ground) and ionic scattering states that arise if the photon energy  $\hbar\omega$  is inserted (instantaneously) into the atom. In a few cases, even interchannel interactions or post-collision effects were taken into account. Apart from the photoemission of just an inner-shell electron, a rearrangement of the residual electron density is likely to occur and leads to a satellite structure to the main photoelectron peaks. Owing to internal correlations, such a rearrangement can give rise to both a monopole or conjugated shake-up of the valence electrons. For the  $1s$  photoionization of Li, the  $R$ -matrix computations of Cheng and co-workers [5] showed that, although this approach is well suited for calculating the conjugated shake-up process, the corresponding intensities were underestimated if the computations are based solely on the overlap integrals of the HF wave functions. For lithium and sodium, moreover, it was shown by Kupliauskiene [24] that a reasonable agreement between the length and velocity forms can be achieved with (nonrelativistic) relaxed orbital calculations if the wave functions of the excited states were constructed orthogonal with regard to lower-lying states of the same symmetry. However, neither the energy dependence of the shake-up intensities nor the branching ratios into higher subshells ( $n \geq 5$ ) were considered in the previous computations.

For all heavier atoms, instead, the theoretical treatment has been more often than not restricted to a simple shake-up model. In this model, the finite probability of an electron to be shaken up to some outer orbital or into the continuum is estimated by the overlap of the one-electron orbitals before and after the photoelectron has left the system. In this picture, the shake-up of an electron is caused by the *sudden* change in the potential. Although this shake-up model includes already a major part of the relaxation, it does not allow one to treat the conjugated shake-up process [25] and often fails even to give reasonable intensities for the normal shake-up lines. In this model, the branching ratio of the satellite and main lines is obtained by normalizing the shake-up probability by the probability of the valence electron to stay in its initial orbital during the ionization. For the inner-shell ionization of rubidium, for example, the branching ratio between the satellite and the main photo line is thus given by  $|\langle ns' | 5s \rangle|^2 / |\langle 5s' | 5s \rangle|^2$ , and it is obvious that this ratio is independent of the photon energy.

Although in the conjugated process the angular momentum unit of the photon is taken over by the ionic core, both the normal and conjugated shake-up are mainly caused by the rearrangement of the bound-state density. In the following, we shall therefore employ separate optimization of the initial and final (bound) states based on the MCDF method. In this method, the dominant relativistic and correlation ef-

fects are taken into account, and only the coupling of the various continuum channels, the so-called interchannel coupling, is neglected right from the beginning.

### A. MCDF method

For open-shell structures as they arise, for example, in the photoionization of inner-shell electrons, the MCDF method has been found a versatile tool to calculate wave functions and cross sections of various kinds [26,27]. In this method [28], an atomic state is approximated by a linear combination of (so-called) configuration-state functions (CSFs) of the same symmetry,

$$|\psi_\alpha(PJM)\rangle = \sum_{r=1}^{n_c} c_r(\alpha) |\gamma_r PJM\rangle, \quad (1)$$

where  $n_c$  is the number of CSFs and  $\{c_r(\alpha)\}$  the representation of the state in the given many-electron basis. In ansatz (1), moreover,  $\gamma_r$  represents the occupation of the atomic shells as well as all further quantum numbers from the coupling of these shells that are required for a unique specification of the  $N$ -electron basis. In most standard computations, the CSFs are constructed as antisymmetrized products of a common set of (orthonormal) orbitals and are optimized by means of the Dirac-Coulomb Hamiltonian. Further relativistic contributions to the representation  $\{c_r(\alpha)\}$  of the atomic states can be added for medium and heavy elements and often help improve their (low-lying) level structure and transition amplitudes. For rubidium and cesium, we therefore included also the low-frequency Breit interaction and vacuum polarization, but left out further corrections [29]. Usually the main limitations of the MCDF model arise for open-shell structures from missing parts in the electronic correlations due to a (restricted) size of the wave-function expansion.

An equivalent but rather different representation of the atomic state vectors is built on an expansion in a determinant basis,

$$|\psi_\alpha(PJM)\rangle = \sum_r^{n_d} d_r(\alpha) |U_{\{u_k\}}^r\rangle, \quad (2)$$

where the Slater determinants

$$|U_{\{u_k\}}\rangle = \frac{1}{\sqrt{N!}} \det\{u_1, \dots, u_N\} \quad (3)$$

are constructed (again) from a given set of orthonormal orbitals  $\{u_k = |n_k \kappa_k m_k\rangle, k=1, \dots, N\}$ . These one-electron functions  $|u_k\rangle$  can be the same orbital as obtained in any relativistic computation; i.e., the  $\langle \vec{r} | u_k \rangle$  may refer also to the Dirac spin-orbitals from the wave function expansion (1) above. Such a determinant basis has been found useful if transition amplitudes are needed between atomic states that are built on two not quite orthogonal sets of one-electron orbitals; cf. Sec. III B. Utilizing the wave functions from the GRASP92 program [30], the representation  $\{d_r(\alpha)\}$  of the atomic-state functions (ASFs) in the determinant basis (2) can be obtained by applying the CESD component [31] from the RATIP program [32].

### B. Photoionization amplitudes including orbital relaxation

In the electric-dipole ( $E1$ ) approximation to the (inner-shell) photoionization, the cross section for obtaining the atom in the final-ionic level  $|\psi_f\rangle \equiv |\psi(P_f J_f)\rangle$  is given by

$$\sigma(P_f J_f) = \frac{4\pi^2 \alpha \omega}{3(2J_i + 1)} \sum_{\kappa_c, J_t} |D(\omega; J_f P_f, \epsilon \kappa_c; J_i P_t)|^2, \quad (4)$$

i.e., by a summation over all possible scattering states of the final system “photoion+electron” that leave the photoion in the state  $|\psi_f\rangle$ . In this notation,  $\alpha$  is the fine-structure constant,  $\hbar\omega$  the photon energy, and  $J_i$  the total angular momentum of the initial (ground) level  $|\psi_i\rangle \equiv |\psi(P_i J_i)\rangle$  of the atom. In Eq. (4), the summation runs especially over all partial waves of the photoelectron with kinetic energy  $\epsilon = E_i + \omega - E_f$  as well as over the allowed continuum states  $|\psi_t\rangle \equiv |J_t P_t, \epsilon \kappa_c; J_i P_t\rangle$  with total angular momentum and parity  $J_t$  and  $P_t$ , respectively.

As seen from Eq. (4), the dipole amplitudes  $D(\omega; J_f P_f, \epsilon \kappa_c; J_i P_t)$  for the transition from the ground state  $|\psi_i\rangle$  to the (total) final state  $|\psi_f\rangle$  form the main building blocks to calculate the relative intensities in the photoelectron spectra. In the  $E1$  approximation, the absorbed photon hereby transfers always the angular momentum  $L=1$  to the total system and also changes the parity of the final state  $|\psi_f\rangle: P_f \neq P_i$ . For the main photopeak, the subshell occupation of the initial and final-ionic levels may just differ by 1, i.e., by the (photo)electron that leaves the atom in the ionization process. However, since the dipole amplitude  $D$  comprises an integration over the coordinates of all electrons, also final-state CSFs with other occupations of the valence shells will give rise in general to nonzero amplitudes. For an independent optimization of the initial- and final-ionic states, these nonzero amplitudes arise mainly from the rearrangement of the electron density in course of the ionization.

Using ansatz (3), its obvious that the computation of the dipole (and many other) amplitudes can be traced back always to the interaction matrix

$$\langle U_{\{u_k\}}^r | D_Q^{(1)} | V_{\{v_l\}}^s \rangle, \quad (5)$$

where  $D_Q^{(1)}$  represents the (rank-1 spherical electric-dipole operator for the) interaction of the atomic electrons with the radiation field. The computation of these amplitudes in the framework of the relativistic theory has been analyzed in detail for the photoionization of an electron in Ref. [33], including the proper phase condition for the emitted electron. The amplitude (5) shows hereby explicitly that the determinants  $|U_{\{u_k\}}\rangle$  and  $|V_{\{v_l\}}\rangle$  need not to be built from the same set of one-electron functions. It is this form of the transition amplitude which has been utilized below in the calculation of the (level-dependent) photoionization cross sections and relative intensities. Expressions for matrix elements  $\langle U_{\{u_k\}} | \hat{A} | V_{\{v_l\}} \rangle$  of general one- and two-particle operators were first derived by Löwdin [34]. In these derivations, it was assumed that  $\langle u_k | u_l \rangle = \langle v_k | v_l \rangle = \delta_{kl}$  is fulfilled for each set of orbitals, but *no* analog relation need apply for the crossed overlap products  $\langle u_k | v_l \rangle = d_{UV}(kl)$ . In particular, we generally have  $\langle u_k | v_l \rangle \neq \langle u_l | v_k \rangle$  due to the different origin of the one-electron functions on the left- and right-hand sides of the

transition amplitudes. This approach was first implemented for the computation of transition probabilities [35] and has now been extended for photoionization processes.

In the computations below, we used the wave functions from the well-known GRASP92 code [30] within the RATIP program [32,36] in order to evaluate all the necessary amplitudes. In particular, we adapted the PHOTO component [27] to account for the nonorthogonality in the computation of the partial and total photoionization cross sections with initial- and final-state orbitals that are not quite orthogonal to each other. For the inner-shell photoionization of medium and heavy elements, such relaxation effects are known to modify the cross sections by up to 30% or even more [37].

### C. Generation of wave functions

In the MCDF model above, it is predominantly the rearrangement of the electron density in course of the inner-shell photoionization that gives rise to a finite shake-up probability for the valence electron. This probability is (nearly) *zero* if the same set of orbitals is utilized for the representation of the initial and final states, and if the electronic correlations are purely handled by means of configuration interaction. Formally, of course, the relaxation of the bound-state density can be obtained also by a sufficient large wave-function expansion, but the size of these expansions would become huge, and the convergence is known to be very slow with regard to changes in the charge density of the inner electrons. Therefore, a pure configuration-interaction approach is unfeasible, and care has to be taken to include the major parts of the electron rearrangement by virtue of a separate optimization of the initial and final atomic states.

Apart from the  $3d^{10}5s^2S_{1/2}$  ground state of rubidium, the final states in the photoionization of a  $3d$  inner-shell electron were generated independently in three different computational models based on ansatz (1): (A) by using all CSF from only the reference configuration  $3d^95s$ , (B) from  $3d^9(5s+6s+5p+4d)$ , and (C) from  $3d^9(5s+6s+5p+4d+7s+6p+5d)$ , respectively. In all these models, the core orbitals for the  $1s, \dots, 4p$  shells were kept frozen [using the one-electron functions from model (A)], and only the  $5s, 6s, \dots$  valence orbitals were reoptimized in the various cases. Indeed, the  $1s, \dots, 4p$  deep-core orbitals remain unaffected if only excitations of the  $5s$  valence electrons are considered, despite the fact that the  $s$  orbitals have a small but finite probability of being near or inside the nucleus. To generate the  $7s$  and  $6p$  functions, moreover, the orbitals from the previous steps needed to be utilized because of convergence failure otherwise. While model (A) just gives rise to the two main peaks (four levels) in the photoelectron spectrum, model (B) accounts for 38 peaks (levels) and the computational model (C) even 72 final levels due to the shake-up of the  $5s$  valence electron. Analogous computations have been carried out also for cesium, but for a  $4d^96s$  reference configuration [model (A)] and by incorporating single-electron excitations into the  $4d^9(6s+7s+6p+5d)$  [for model (B)], and  $4d^9(6s+7s+6p+5d+8s+7p+6d)$  [for model (C)], respectively. Although such a limited expansion does not enable one to “monitor” the convergence of the photoionization cross sections into

the various shake-up levels, it takes into account a major part of the relaxation and enables us to investigate the intensity ratios as function of the photon energy.

## IV. RESULTS AND DISCUSSION

In the alkali-metal atoms, the photoionization of an  $nd$  inner-shell electron gives rise to two main peaks due to the spin-orbit splitting of the  $nd_{3/2,5/2}$  subshells—i.e., the occurrence of a  $nd_{3/2}$  and  $nd_{5/2}$  hole together with a  $ms$  valence electron. In rubidium, for example, these peaks refer to the  $3d_{3/2}^{-1}5s(J=1,2)$  and  $3d_{5/2}^{-1}5s(J=2,3)$  final levels of the photoion and are separated in energy by about 1.5 eV from each other. The fine-structure splitting due to the coupling of the valence electron with the inner-shell hole cannot be resolved because of the natural lifetime broadening of these  $nd^{-1}$  hole states. In a simple statistical model, the main peaks are therefore expected to show an intensity ratio of 2:3. At the low-kinetic-energy side, these peaks are associated with their satellites in which the outer  $s$  electron is “shaken” into some higher orbital of either the same (normal) or different angular momentum (conjugated shake). Owing to the high resolution in the electron spectra, it is possible today to isolate not only excitations of the  $ms$  electrons into the neighbored  $(m+1)s$  and  $mp$  shells, but to resolve also a number of other satellites.

### A. Rb $3d \rightarrow n'l'$ satellite spectrum

Figure 1 shows the Rb  $3d^{-1}nl$  photoelectron spectrum, measured at the photon energy of 200 eV in the region well above the ionization threshold [10]. This spectrum has been recorded at the magic angle of  $54.7^\circ$  relative to the polarization vector of the incoming photons. Apart from the two main photopeaks (12 and 13 in Fig. 1), more than ten satellite peaks can clearly be resolved from the photoelectron spectrum and are assigned to final-state configurations of the photoion as shown in Table I. The assignment of the peaks has been made due to the occupation of the valence electrons, and an overlay of several configurations is found only in a very few cases (cf. peaks 4 and 11). Beside the assignment, Table I also displays the binding energies and the relative intensities of the photopeaks, normalized on the  $3d_{5/2}^{-1}5s$  dominant peak. The intensity ratio of the main peaks (12 and 13) agrees well with the statistical ratio 0.67, which suggests that the mixing between the  $3d^{-1}5s$  and  $3d^{-1}4d$  configurations is small. On the other hand, the ratio differs by about 1.6% from the statistical expectation. The orbital relaxation can explain this deviation as shown by a nearly perfect agreement between the experiment and theory in columns 4, 6, and 8 in Table I.

Although the main contribution to the photoelectron satellites arises from the  $5s \rightarrow 6s$  monopole excitations, the conjugated  $5p$  satellites also receive a quite remarkable intensity, which is suppressed only by a factor of 3. A similar ratio is found also for the  $7s$  and  $6p$  satellites. To understand this spectrum, the relative intensities of the photosatellites have been calculated in a number of models. In the standard shake model (column 5 in Table I)—that is, based simply on the

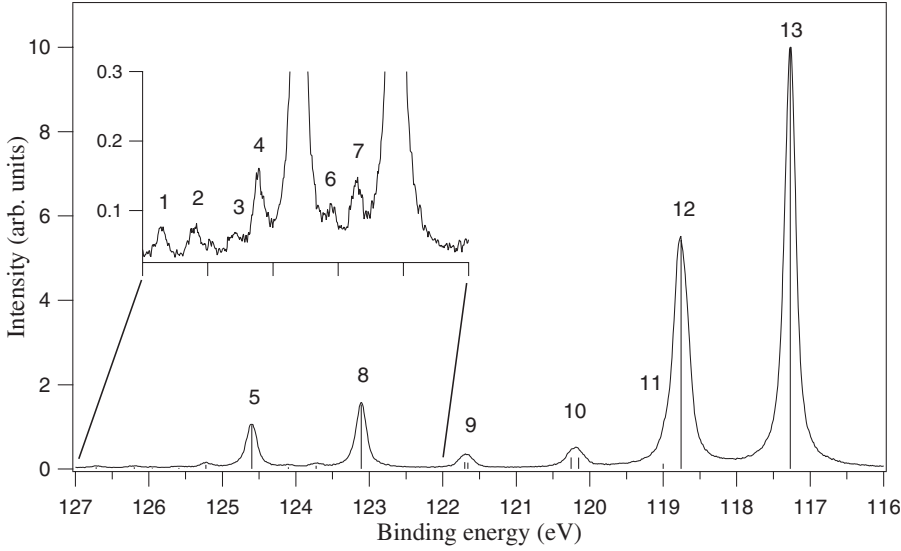


FIG. 1. Experimental  $3d_{3/2,5/2}^{-1}5s$  photoelectron peaks (12 and 13) of atomic rubidium together with  $3d_{3/2,5/2}^{-1}nl$  shake-up satellite structures (reprinted from Ref. [10]). See Table I for an assignment of the electron peaks in terms of the final-state configuration of the photoion.

overlap of the  $5s$  valence electron—only monopole excitations into the  $6s$  and  $7s$  shells are allowed, and this contribution is overestimated both for the  $5s \rightarrow 6s$  and  $5s \rightarrow 7s$  satellites. In the computational models described in Secs. III B and III C, in contrast, no distinction needs to be made between the monopole and conjugated shake-up lines since the proper transfer of the internal angular momentum is ensured by calculating the full many-electron amplitudes. In columns 6 and 7 of Table I, the relative intensities of the  $3d^{-1}$  photoelectron lines are shown if calculated with the wave function expansions from models (B) and (C). A clear improvement is seen especially for the two  $3d^{-1}6s$  peaks. In the last column,

we reoptimized in addition the  $3d$  inner-shell electron while the other orbitals were kept fixed due to their generation in model (C). Hereby, all photoionization amplitudes and cross sections have been calculated in length gauge. Good agreement between experiment and computations is found, especially for the computational models from the last two columns. The agreement is somewhat weaker for the  $3d^{-1}5p$  conjugated photopeaks, which are overestimated by about 50% and by almost a factor of 3 for the  $3d^{-1}6p$  peaks. Of course, these conjugated shake-up lines are more sensible to details in the computational procedure than the normal shake-up transitions, and it can be expected, moreover, that

TABLE I. Energies and relative intensities of the  $3d^{-1}$  photoelectron lines of rubidium. The assignment of the electron peaks refers to the final configuration of the photoion following the photoionization of a  $3d$  inner-shell electron.

Label	Assignment	Experiment		Calculation			
		Binding energy (eV) [10]	Int. [10]	Int. <sup>a</sup>	Int. <sup>b</sup>	Int. <sup>c</sup>	Int. <sup>d</sup>
1	$3d_{3/2}^{-1}7s_{1/2}$	126.7(1)	$0.42 \pm 0.1$	1.06		0.48	0.49
2	—	126.2(1)	$0.42 \pm 0.1$				
3	$3d_{3/2}^{-1}6p_{1/2,3/2}$	125.6(1)	$0.27 \pm 0.1$			1.09	1.10
4	$3d_{5/2}^{-1}7s_{1/2} + 3d_{3/2}^{-1}5d_{3/2,5/2}$	125.2(1)	$1.01 \pm 0.2$	1.59		0.72	0.74
5	$3d_{3/2}^{-1}6s_{1/2}$	124.60(5)	$10.39 \pm 0.3$	12.58	13.15	10.01	10.19
6	$3d_{5/2}^{-1}6p_{1/2,3/2}$	124.1(1)	$0.45 \pm 0.1$			1.70	1.71
7	$3d_{5/2}^{-1}5d_{3/2,5/2}$	123.7(1)	$0.78 \pm 0.2$			0.06	0.06
8	$3d_{5/2}^{-1}6s_{1/2}$	123.11(5)	$15.29 \pm 0.4$	18.87	19.50	14.87	15.13
9	$3d_{3/2}^{-1}5p_{1/2,3/2}$	121.7(1)	$3.22 \pm 0.2$		6.01	5.69	5.68
10	$3d_{5/2}^{-1}5p_{1/2,3/2}$	120.2(1)	$5.51 \pm 0.4$		9.35	8.83	8.81
12 (11)	$3d_{3/2}^{-1}5s_{1/2}(3d_{5/2}^{-1}4d_{3/2,5/2})$	118.76(5)	$65.58 \pm 0.8^c$	66.67	65.55	66.30	65.51
13	$3d_{5/2}^{-1}5s_{1/2}$	117.27(5)	100	100	100	100	100

<sup>a</sup>Applying the overlaps in the standard shake model.

<sup>b</sup>Relaxed-orbital calculations for a photon energy of 200 eV, using wave function from the computational model B.

<sup>c</sup>Same as in footnote b, but with wave functions from model (C).

<sup>d</sup>Same as in footnote c, but by reoptimizing also the  $3d$  orbital.

<sup>e</sup>Corrected for a misprint (55.58) in Ref. [10].

these lines are affected by interactions within the continuum (which are omitted in the present computations). Again, however, the agreement improves in going from model (B) to the more extensive computational model (C) for the wave-function expansions. This indicates that a slightly better agreement might be obtained by using even larger basis sets. As seen from the calculated intensities for peak 7, almost no intensity is transferred into the  $5d$  shells, which is caused, very likely, by the fact that only single excitations are taken into account in all wave functions. For a better description of the  $5s \rightarrow 5d$  satellites, at least double excitations from the  $3d^9 5s$  reference configuration to the  $3d^9 4s^2 4p^4 4d^2 5s$  and  $3d^9 4s^2 4p^4 5s 5d^2$  are likely required, since relaxation alone without some proper configuration interaction cannot transfer intensity from the  $s \rightarrow d$  symmetry in the evaluation of the photoionization amplitudes. Similar arguments might apply also for the  $3d^{-1} 5p$  and  $3d^{-1} 6p$  conjugated shake-up lines and might lead to a reduction in the corresponding intensities.

### B. Energy-dependent branching ratios

If differences in the radial structure of the  $3d_{3/2}$  and  $3d_{5/2}$  orbitals are neglected (as well as further many-electron effects), the two main photopeaks 12 and 13 should have a statistical ratio 2:3. This ratio is expected for sufficient large photon energies and is, indeed, well fulfilled by experiment and for computations with photon energy  $h\nu \geq 200$  eV. This shows that pure fine-structure effects are not so important for the electron-photon interaction if the energy, deposited into the system, reaches far above its ionization threshold. For the main  $3d_{5/2}^{-1} 5s$  and  $3d_{3/2}^{-1} 5s$  photopeaks, these thresholds are 117.27 eV and 118.76 eV, respectively. To explore the intensity ratios of the main and satellite lines as a function of the (total) energy of the atom+photon system, they have been recorded at several photon energies in the region  $h\nu = 134$ – $220$  eV. Figures 2(a)–2(c) compare the experimental and theoretical intensity ratios for different satellite lines as function of the photon energy. For the guidance of the reader, moreover, Fig. 2(d) displays the corresponding photoelectron spectrum at  $h\nu = 200$  eV. A rather different behavior is found for the intensity ratios of the normal and conjugated shake-up lines. While the  $3d_j^{-1} 6s/3d_j^{-1} 5s$  ( $j=3/2, 5/2$ ) intensity ratios slowly increase with photon energy (but are almost independent of energy as predicted by the simple shake-up model, based on the  $|\langle 6s_{\text{final}} | 5s_{\text{initial}} \rangle|^2$  overlap), the intensity ratio of the  $3d_j^{-1} 5p/3d_j^{-1} 5s$  conjugated-to-normal lines decreases by about a factor of 2 in going from 134 eV to 220 eV. In particular, the calculated  $3d_j^{-1} 5p/3d_j^{-1} 5s$  intensity ratio occurs as being very sensitive with regard to the photon energy and overestimates the observed ratio by a factor of 3 (or more) close to the threshold. For rubidium, this intensity ratio has been measured here as a function of the photon energy, and our computational model (B) is at least able to predict the trend of this  $5s \rightarrow 5p$  conjugated shake-up line reasonably well. Good agreement with experiment is found for this ratio only at high photon energies. As expected from previous case studies for Li [5], therefore, such conjugated-to-normal intensity ratios

provide an excellent test bed for all many-electron computations on the inner-shell photoionization of atoms and ions.

Correlations in many-electron atoms are responsible for the satellite structure in the photoelectron spectrum, but they are not the only reason for the energy dependence of the individual lines and line ratios. In particular, the  $3d_{3/2}^{-1} 5s/3d_{5/2}^{-1} 5s$  intensity ratio of the two main peaks in Fig. 2(c) depends only very little on the relaxation of the electron density (cf. Table I), but rather on the energy dependence of the photoionization cross sections. The decrease of this intensity ratio from the statistical value  $2:3=0.6\bar{6}$ – $0.54$ , as observed in the measurements, is caused mainly by the behavior of the  $3d_{3/2}^{-1} 5s$  and  $3d_{5/2}^{-1} 5s$  cross sections at low photon energies. Similar arguments may hold also for the  $3d_j^{-1} 6s/3d_j^{-1} 5s$  intensity ratios, but the situation is here more involved due to the different ionization thresholds of the main and satellite lines, and the fact that the photoionization cross sections do not decrease linearly with the photon energy.

### C. Cs $4d \rightarrow n'l'$ satellite spectrum

Analogous computations as for rubidium have been carried out also for cesium—i.e., the next heavier alkali metal with nuclear charge  $Z=55$ —and for the inner-shell photoionization of a  $4d$  electron. The experimental  $4d$  photoelectron spectrum of Cs, measured at the photon energy of 142.5 eV, is shown in Fig. 3. The corresponding assignment of the peaks together with calculated values for their binding energies and relative intensities is displayed in Table II. Apart from the  $4d^{-1} 6s$  main photoelectron peaks, the satellites are resolved and assigned up to the  $4d^{-1} 8p$  shake-up lines. Note that the binding energies of these peaks are slightly underestimated in Table II by about 1.2–0.3 eV, which reflects a  $5p^6 6s^2 S_{1/2}$  ground state that is not enough correlated within the applied computational basis. A better description of the ground (and excited) states is usually achieved if single and double excitation of the  $5p$  and  $6s$  (sub)valence electrons into the  $4f$ ,  $5d$ ,  $6p$ , and  $7s$  shells would be taken into account, but which is beyond the scope of the present work. For the  $4d^{-1}(7p+7d+8s)$  shake-up lines, the difference between the experimental and theoretical excitation (binding) energies becomes less pronounced since these higher-excited levels can also not be represented so well in the computations.

Photoabsorption of the  $4d$  shell of Cs has been studied in various articles (see, e.g., Ref. [38] and references therein), but to the best of our knowledge, the  $4d$  photoionization satellites have been studied so far only by Mäntykenttä *et al.* [20] with moderate experimental resolution. In that study, just two satellite lines were resolved (which correspond to peaks 6 and 11 in Fig. 3) and assigned to the  $6s \rightarrow 7s$  monopole shake-up. As shown in Fig. 3, however, these two lines overlap with other satellite lines and, hence, lead to an overestimation of the  $6s \rightarrow 7s$  shake-up probabilities if only a moderate resolution is obtained for the electron spectra. In Ref. [11], the  $6s \rightarrow 7s$  shake-up probability was therefore corrected to some smaller value, but any further analysis of the satellite spectrum was omitted up to the present.

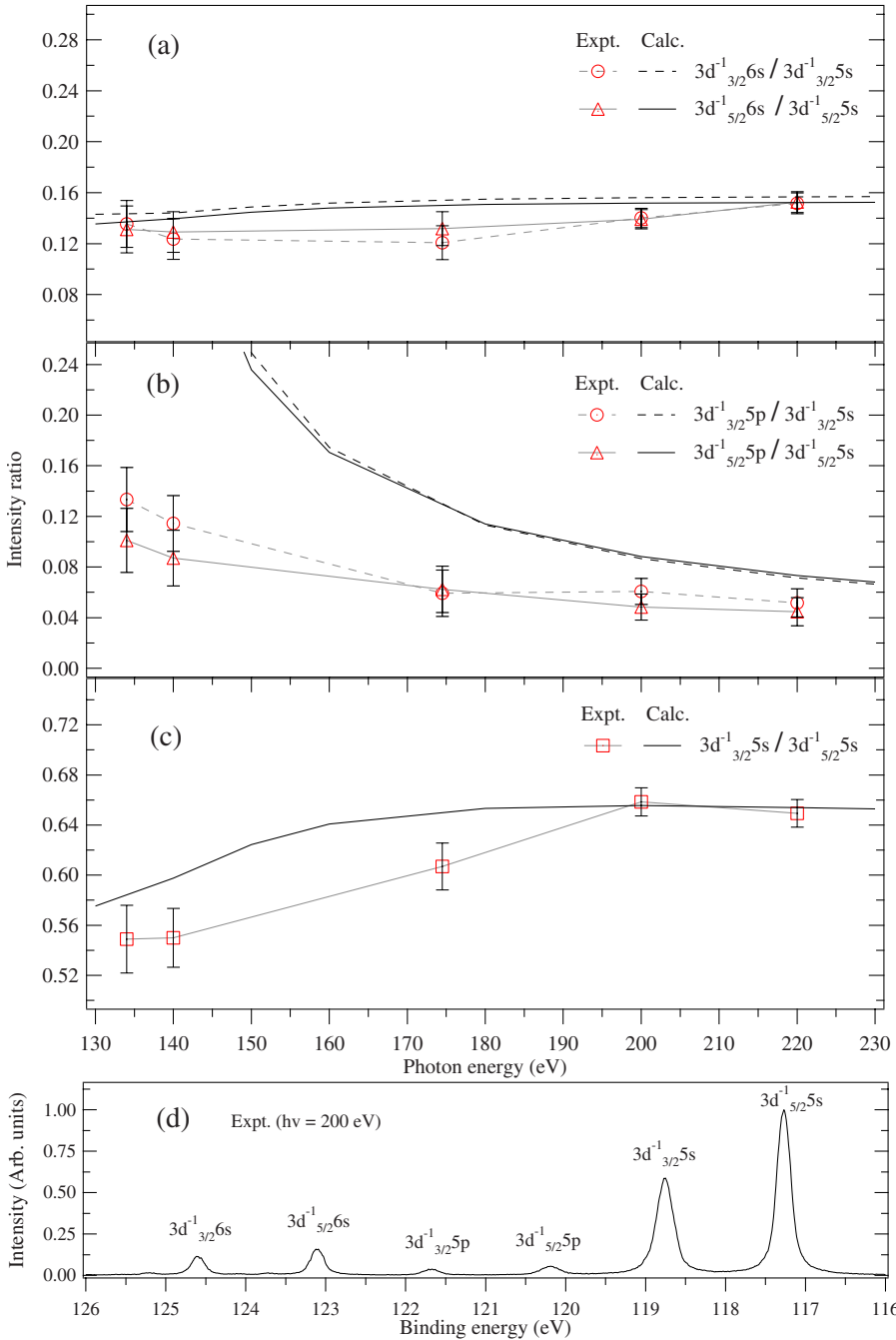


FIG. 2. (Color online) Comparison of different experimental and theoretical intensity ratios as function of the photon energy between 134 and 220 eV. (a)  $3d_{j=3/2}^{-1}6s / 3d_{j=3/2}^{-1}5s$ , (b)  $3d_{j=3/2}^{-1}5p / 3d_{j=3/2}^{-1}5s$ , and (c)  $3d_{3/2}^{-1}5s / 3d_{5/2}^{-1}5s$ . The computational model (B) has been utilized. For the guidance of the reader, panel (d) displays the intensities of the selected photopeaks at the photon energy  $h\nu=200$  eV.

Of course, cesium has a very similar valence-shell structure as rubidium, but with completely filled  $4d$ ,  $5s$ , and  $5p$  shells in addition to the  $6s$  valence electron. When compared with the  $3d$  electrons in rubidium, the  $4d$  electrons in cesium have a binding energy that is lower by about 35 eV. This reduction can be easily understood from the screening of the  $4d$  orbitals in cesium, which give rise to the mean radius  $\langle r \rangle \approx 0.8$  a.u. This mean radius has to be compared with  $\langle r \rangle \approx 0.5$  a.u. for the  $3d_{3/2,5/2}$  orbitals of Rb. This different screening behavior already suggests that cesium must be expected to be more sensitive with regard to correlation effects as seen, for example, from the peaks for Cs (cf. 14-15 and 19-20 in Fig. 3) that all arise from the mixing of the  $4d^{-1}6s$  and  $4d^{-1}5d$  configurations, while only a single peak (No. 11 in Table I) was assigned to the corresponding  $3d^{-1}5s$  and

$3d^{-1}4d$  mixing in Rb. Moreover, since the relaxation of the  $d$  orbitals is in Cs smaller than in Rb, the monopole shake-up probabilities are also smaller in this case. On the other hand, the conjugated shake-up probabilities stay approximately the same. For cesium, of course, the relativistic effects are much stronger, and this applies even for the ( $6s$ ) valence electron. In fact, relativity arises here for three reasons for the valence shells: (i) the spin-orbit splitting of all orbitals with orbital angular momentum  $l \geq 1$ , (ii) the relativistic contraction of the inner electrons that gives rise to a larger screening for the valence electrons (the so-called “indirect” relativistic effect), and (iii) since especially the  $s$  electrons have a finite probability near (or within) the nucleus. The latter reason mainly influences the radiative corrections to the level energies and remains small for cesium as a mid- $Z$  element. However, the

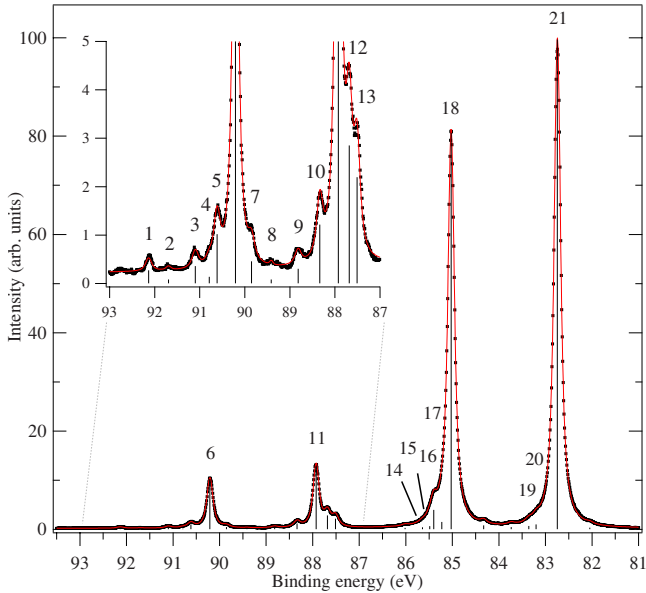


FIG. 3. (Color online) Experimental  $4d_{3/2,5/2}^{-1}6s$  photoelectron peaks (19 and 24) of atomic cesium together with the  $4d_{3/2}^{-1}nl$  and  $4d_{5/2}^{-1}nl$  shake-up satellite structures. The spectrum was measured at the photon energy of 142.5 eV. For better visibility, the binding energy region between 87 and 93 eV is magnified. Fitted peaks without numbering are identified as overlapping Auger electron lines.

spin-orbit splitting is well visible also for the  $6s \rightarrow 6p$  satellite lines to which the peaks 12-13 and 17-18 are assigned. For these peaks, the spin-orbit coupling of the  $6p$  electron divides the main photolines due to the  $4d_{3/2}^{-1}6p_j$  and  $4d_{5/2}^{-1}6p_j$  relativistic configurations further because of the splitting of the  $6p_{1/2}$  and  $6p_{3/2}$  valence orbitals. As seen from Table II, our calculations for the  $6s \rightarrow 6p$  conjugated shake-up probabilities agree well with the experiment. Note that this agreement is better than for the  $5s \rightarrow 5p$  conjugated shake-up of Rb, although it might occur here somewhat accidentally.

To describe the excitation of the  $6s$  valence electron in cesium appears to be a rather sophisticated task. The orbitals with  $n > 6$  tend to be quite diffuse, and layers of even higher- $n$  Rydberg orbitals are needed to correct for the representation of the valence electrons at lower  $n$ . This all leads to convergence problems in the computation of additional valence orbitals and often enforces one to “freeze” some of the orbital in the SCF procedure. These difficulties can be seen, for example, from the comparison of the calculated and experimental  $6s \rightarrow 7s$  and  $6s \rightarrow 8s$  shake-up probabilities. While the  $6s \rightarrow 7s$  probability is overestimated and very sensitive to the orbital optimization (cf. columns 6 and 7 in Table II), the  $6s \rightarrow 8s$  shake-up probability is clearly underestimated. This implies that the  $8s$  orbital does not collapse enough in our calculations. The different behavior of the valence shells in Cs, when compared to those of rubidium, becomes visible also for the  $4d_{3/2}^{-1}6s/4_{5/2}^{-1}6s$  branching ratio of the main lines that clearly deviate from the statistical ratio 2:3. This deviation is likely caused by the shape resonance that starts at the  $4d$  ionization threshold and continues to about 100 eV above the threshold. This shape resonance is well understood in the  $4d$  photoionization of Xe (see, e.g.,

Ref. [39]), and a further analysis of this resonance for the case of Cs is beyond the scope of this work. Our calculations indicate, however, that the  $4d_{3/2}^{-1}6s/4_{5/2}^{-1}6s$  branching ratio will return to its statistical value at around 200 eV above the ionization threshold. Unfortunately, the cross sections at these energies are unfeasibly small for high-resolution measurements of such small satellite structures.

It is interesting to note that the shape resonance also affects the branching ratios between the spin-orbit splitted satellite lines. For example, the experimental  $4d_{3/2}^{-1}7s/4d_{5/2}^{-1}7s$  ratio of 0.806 is very close to the  $4d_{3/2}^{-1}6s/4d_{5/2}^{-1}6s$  ratio of 0.801 that applies for the two main lines.

For the conjugated shake-up in the  $4d^{-1}5d$  levels, the predicted intensity is too small for cesium and arises mainly from configuration mixing, similar as for the  $5s \rightarrow 4d$  excitation of rubidium. Again, double excitations from the  $4d^{-1}6s$  reference configuration into the  $4d^0 5s^2 5p^4 5d^2 6s$  and  $4d^0 5s^2 5p^4 5s 6d^2$  configurations are likely to be required in order to describe these line intensities properly. Overall, however, these probabilities remain overall rather small when compared with the main  $4d_{5/2}^{-1}6s$  photopeak. Further theoretical work is therefore needed to predict the intensities also of the  $nl \rightarrow n'(l+2)$  photosatellites.

## V. CONCLUSIONS

The photoelectron satellite structure of rubidium and cesium has been investigated following the photoionization of a  $3d$  and  $4d$  inner-shell electron, respectively. Emphasis in these studies has been placed especially on the intensity ratios of the  $nd^{-1}ms$  monopole and  $nd^{-1}m'p$  conjugated satellite lines that have been measured with high-resolution electron spectroscopy at MAX-lab and are compared with relativistic MCDHF computations. A reasonable agreement between experiment and computations is found, for both the monopole and conjugated shake-up probabilities, if the relaxation of the bound-state electron density is taken into account in the evaluation of the photoionization amplitudes. To demonstrate the capability of the method for medium and heavy elements, calculations were carried out for the shake-up satellites up to the  $7s$  and  $6p$  shells for Rb and the  $8s$ ,  $7p$ , and  $7d$  shells for Cs. In addition to the intensity ratios, the photon energy dependence of the most intense satellites was studied for rubidium. For cesium, moreover, the  $4d$  photoelectron and satellite spectrum was recorded with a previously unmatched high resolution that enables us to assign and classify 21 new satellite peaks from the spectrum.

In particular for mid- $Z$  elements such as Rb and Cs, a large fraction of the shake-up probability seems to arise from the orbital relaxation. If this rearrangement of the bound-state density is included already in the evaluation of the photoionization amplitudes, no distinction need be made between the monopole and conjugated shake-up satellites in the photoelectron spectra, although the latter one remains slightly more sensitive to many-particle and, probably, also continuum-interaction effects. Apart from the energy ratios for fixed photon energies, this method is able also to describe the energy dependence for both the  $nl \rightarrow n'l$  monopole and

TABLE II. Energies and relative intensities of the  $4d^{-1}$  photoelectron lines of cesium. The assignment of the electron peaks refers to the final configurations following the photoionization of the  $4d$  inner-shell electron.

Label	Assignment	Experiment		Calculation		
		Energy (eV)	Intensity	Energy (eV)	Int. <sup>a</sup>	Int. <sup>b</sup>
1	$4d_{3/2}^{-1}8s_{1/2}$	92.1(1)	$0.27 \pm 0.1$	91.64	0.12	0.11
2	$4d_{3/2}^{-1}7d_{3/2,5/2}$	91.7(1)	$0.06 \pm 0.1$			
3	$4d_{3/2}^{-1}7p_{1/2,3/2}$	91.1(1)	$0.36 \pm 0.1$	89.76	0.81	0.58
4	$4d_{5/2}^{-1}8p_{1/2,3/2}$	90.8(2)	$0.14 \pm 0.1$			
5	$4d_{5/2}^{-1}6d_{3/2,5/2}$	90.6(2)	$1.01 \pm 0.2$	89.37	0.007	0.009
6	$4d_{3/2}^{-1}7s_{1/2}$	90.21(5)	$9.53 \pm 0.7$	88.91	14.79	11.22
7	$4d_{5/2}^{-1}8s_{1/2}$	89.9(2)	$0.46 \pm 0.1$	89.38	0.15	0.14
8	$4d_{5/2}^{-1}7d_{3/2,5/2}$	89.4(1)	$0.04 \pm 0.1$			
9	$4d_{5/2}^{-1}7p_{1/2,3/2}$	88.8(1)	$0.31 \pm 0.1$	87.51	1.27	0.90
10	$4d_{5/2}^{-1}6d_{3/2,5/2}$	88.3(1)	$1.22 \pm 0.2$	87.08	0.007	0.006
11	$4d_{5/2}^{-1}7s_{1/2}$	87.93(5)	$11.82 \pm 0.8$	86.65	19.53	14.82
12	$4d_{5/2}^{-1}6p_{3/2}$	87.7(1)	$2.84 \pm 0.4$	86.40	1.68	1.59
13	$4d_{3/2}^{-1}6p_{1/2}$	87.5(1)	$2.18 \pm 0.5$	86.56	1.70	1.60
14	$4d_{3/2}^{-1}5d$	85.6(2)	$0.41 \pm 0.1$			
15	$4d_{3/2}^{-1}5d$	85.5(2)	$0.66 \pm 0.1$			
16	$4d_{5/2}^{-1}6p_{3/2}$	85.4(1)	$3.97 \pm 0.5$	84.32	2.75	2.59
17	$4d_{5/2}^{-1}6p_{1/2}$	85.2(1)	$1.52 \pm 0.9$	84.29	2.48	2.35
18	$4d_{3/2}^{-1}6s_{1/2}$	85.03(5)	$80.13 \pm 1.1$	84.17	75.99	75.98
19	$4d_{5/2}^{-1}5d$	83.4(2)	$0.70 \pm 0.1$			
20	$4d_{5/2}^{-1}5d$	83.2(2)	$1.02 \pm 0.1$			
21	$4d_{5/2}^{-1}6s_{1/2}$	82.74(5)	100.00	81.92	100.00	100.00
	$\Sigma 4d_{3/2}^{-1}5d$		1.07		0.07	0.07
	$\Sigma 4d_{5/2}^{-1}5d$		1.72		0.12	0.12

<sup>a</sup>Relaxed-orbital calculations for the photon energy of 142.5 eV, using wave function from the computational model (C).

<sup>b</sup>Same as in footnote a, but by reoptimizing the  $4d$  orbital.

$nl \rightarrow n'(l+1)$  conjugated satellite lines. However, further work is required for a description of the  $ns \rightarrow n'd$  ( $n=5,6$ ;  $n'=4,5,6$ ) photosatellites that are clearly underrated in the present work.

#### ACKNOWLEDGMENTS

The work has been financially supported by the Research Council for Natural Sciences of the Academy of Finland and the European Community-Research Infrastructure Action un-

der the FP6 "Structuring the European Research Area" Program (through the Integrated Infrastructure Initiative "Integrating Activity on Synchrotron and Free Electron Laser Science"). K.J. acknowledges financial support from the Vilho, Yrjö and Kalle Väisälä Foundation. S.U. was financed by the Marie Curie Early Stage Training Site MAXLAS (Grant No. MEST-CT-2005-020356) within the 6th European Community Framework Program. We thank also the staff of MAX-laboratory for their kind help during the experiments.

- |  |   |
|--|---|
| <p>[1] D. Cubaynes, J. M. Bizau, F. J. Wuilleumier, B. Carre, and F. Gounand, Phys. Rev. Lett. <b>63</b>, 2460 (1989).</p> <p>[2] J. M. Bizau, P. Gérard, F. J. Wuilleumier, and G. Wendin, Phys. Rev. A <b>36</b>, 1220 (1987).</p> <p>[3] D. Cubaynes, E. Heinecke, T. Richter, S. Diehl, F. J. Wuilleumier, P. Zimmermann, and M. Meyer, Phys. Rev. Lett. <b>99</b>, 213004 (2007).</p> | <p>[4] B. Langer, J. Viefhaus, O. Hemmers, A. Menzel, R. Wehlitz, and U. Becker, Phys. Rev. A <b>43</b>, 1652 (1991).</p> <p>[5] W. T. Cheng, E. Kukk, D. Cubaynes, J.-C. Chang, G. Snell, J. D. Bozek, F. J. Wuilleumier, and H. Berrah, Phys. Rev. A <b>62</b>, 062509 (2000).</p> <p>[6] D. Cubaynes, L. Voky, F. J. Wuilleumier, B. Rouvellou, A. Hibbert, P. Faucher, J.-M. Bizau, L. Journal, H. E. Saraph, and</p> |
|--|---|

- F. Bely-Dubau, *Phys. Rev. A* **57**, 4432 (1998).
- [7] G. Snell, M. Martins, E. Kukk, W. T. Cheng, and N. Berrah, *Phys. Rev. A* **63**, 062715 (2001).
- [8] T. Richter, E. Heinecke, P. Zimmermann, K. Godehusen, M. Yalcinkaya, D. Cubaynes, and M. Meyer, *Phys. Rev. Lett.* **98**, 143002 (2007).
- [9] K. Jänkälä, R. Sankari, J. Schulz, M. Huttula, A. Calo, S. Heinäsmäki, S. Fritzsche, T. Rander, S. Svensson, S. Aksela, and H. Aksela, *Phys. Rev. A* **73**, 022720 (2006).
- [10] K. Jänkälä, J. Schulz, M. Huttula, A. Calo, S. Urpelainen, S. Heinäsmäki, S. Fritzsche, S. Svensson, S. Aksela, and H. Aksela, *Phys. Rev. A* **74**, 062704 (2006).
- [11] K. Jänkälä, J. Schulz, and H. Aksela, *J. Electron Spectrosc. Relat. Phenom.* **161**, 95 (2006).
- [12] K. Jänkälä, S. Fritzsche, M. Huttula, J. Schulz, S. Urpelainen, S. Heinäsmäki, S. Aksela, and H. Aksela, *J. Phys. B* **40**, 3435 (2007).
- [13] G. Mehlman, J. W. Cooper, and E. B. Saloman, *Phys. Rev. A* **25**, 2113 (1982).
- [14] L. VoKy, P. Faucher, A. Hibbert, J. M. Li, Y. Z. Qu, J. Yan, J. C. Chang, and F. Bely-Dubau, *Phys. Rev. A* **57**, 1045 (1998).
- [15] D. Cubaynes, S. Diehl, L. Journel, B. Rouvellou, J.-M. Bizau, S. Al Moussalami, F. J. Wuilleumier, N. Berrah, L. VoKy, P. Faucher, A. Hibbert, C. Blancard, E. Kennedy, T. J. Morgan, J. Bozek, and A. S. Schlachter, *Phys. Rev. Lett.* **77**, 2194 (1996).
- [16] J. W. Cooper, *Phys. Rev. A* **59**, 4825 (1999).
- [17] F.-C. Chen, J.-L. Wu, S. S. Yang, K.-H. Hsieh, and W.-C. Chen, *J. Appl. Phys.* **103**, 103721 (2008).
- [18] R. M. Cornell, *J. Radioanal. Nucl. Chem.* **171**, 483 (1993).
- [19] M. Huttula, S. Heinäsmäki, H. Aksela, E. Kukk, and S. Aksela, *J. Electron Spectrosc. Relat. Phenom.* **156-158**, 270 (2007).
- [20] A. Mäntykenttä, H. Aksela, S. Aksela, A. Yagishita, and E. Shigemasa, *J. Phys. B* **25**, 5315 (1992).
- [21] N. M. Kabachnik, S. Fritzsche, A. N. Grum-Grzhimailo, M. Meyer, and K. Ueda, *Phys. Rep.* **451**, 155 (2007).
- [22] C. G. King, M. Tronc, F. H. Read, and R. C. Bradford, *J. Phys. B* **10**, 2479 (1977).
- [23] A. Kivimäki, L. Pfeiffer, H. Aksela, E. Nömmiste, and S. Aksela, *J. Electron Spectrosc. Relat. Phenom.* **101-103**, 43 (1999).
- [24] A. Kupliauskiene, *J. Phys. B* **32**, 3939 (1999).
- [25] There have been used various terms in the literature to denote the conjugated shake-up process, such as inelastic scattering, direct knock-out, or interchannel coupling. Here, we make use of the term “conjugated shake-up” in order to emphasize the close phenomenological relation to normal shake-up.
- [26] S. Fritzsche, *Phys. Scr.* **T100**, 37 (2002).
- [27] S. Fritzsche, J. Nikkinen, S.-M. Huttula, H. Aksela, M. Huttula, and S. Aksela, *Phys. Rev. A* **75**, 012501 (2007).
- [28] I. P. Grant, in *Methods in Computational Chemistry*, Vol. 2, edited by S. Wilson (Plenum Press, New York, 1988), p. 1.
- [29] S. Fritzsche, C. Froese Fischer, and G. Gaigalas, *Comput. Phys. Commun.* **148**, 103 (2002).
- [30] F. A. Parpia, C. Froese Fischer, and I. P. Grant, *Comput. Phys. Commun.* **94**, 249 (1996).
- [31] S. Fritzsche and I. P. Grant, *Comput. Phys. Commun.* **92**, 111 (1995).
- [32] S. Fritzsche, *J. Electron Spectrosc. Relat. Phenom.* **114-116**, 1155 (2001).
- [33] S. Fritzsche, A. Surzhykov, and T. Stöhlker, *Phys. Rev. A* **72**, 012704 (2005).
- [34] P. O. Löwdin, *Phys. Rev.* **97**, 1474 (1955).
- [35] S. Fritzsche, C. Froese Fischer, and C. Z. Dong, *Comput. Phys. Commun.* **124**, 340 (2000).
- [36] S. Fritzsche, H. Aksela, C. Z. Dong, S. Heinäsmäki, and J. E. Sienkiewicz, *Nucl. Instrum. Methods Phys. Res. B* **205**, 93 (2003).
- [37] M. Kutzner and V. Radojevic, *Phys. Rev. A* **49**, 2574 (1994).
- [38] A. Cummings, C. McGuinness, G. OSullivan, J. T. Costello, J. P. Mosnier, and E. T. Kennedy, *Phys. Rev. A* **63**, 022702 (2001).
- [39] A. Ausmees, S. J. Osborne, R. Moberg, S. Svensson, S. Aksela, O.-P. Sairanen, A. Kivimäki, A. Naves de Brito, E. Nömmiste, J. Jauhiainen, and H. Aksela, *Phys. Rev. A* **51**, 855 (1995).